applied sciences

MDPI

Article

In Silico Study and Excito-Repellent Activity of *Vitex negundo* L. Essential Oil against *Anopheles gambiae*

Bamidele J. Okoli [1,*], Wafa Ali Eltayb [2], Gideon A. Gyebi [3], Amr R. Ghanam [4], Zakari Ladan [5], Joseph C. Oguegbulu [1] and Mohnad Abdalla [2,6,*]

1 Department of Chemical Sciences, Faculty of Science and Technology, Bingham University, Karu 961105, Nasarawa State, Nigeria; joseph.oguegbulu@binghamuni.edu.ng
2 Biotechnology Department, Faculty of Science and Technology, Shendi University, Shendi 11111, Nher Anile, Sudan; wafa.ali.11338@gmail.com
3 Department of Biochemistry, Faculty of Science and Technology, Bingham University, Karu 961105, Nasarawa State, Nigeria; gideonagyebi@gmail.com
4 Department of Medicine, Vascular Biology Center, Medical College of Georgia at Augusta University, Augusta, GA 30912, USA; amr@mail.ustc.edu.cn
5 Department of Pure and Applied Chemistry, Faculty of Science, Kaduna State University, Kaduna 800283, Kaduna State, Nigeria; zakari.ladan@kasu.edu.ng
6 Key Laboratory of Chemical Biology, Ministry of Education, Department of Pharmaceutics, School of Pharmaceutical Sciences, Cheeloo College of Medicine, Shandong University, 44 Cultural West Road, Jinan 250012, China
* Correspondence: okolibj@binghamuni.edu.ng (B.J.O.); mohnadabdalla200@gmail.com (M.A.); Tel.: +234-8039615649 (B.J.O.)

Abstract: (1) Background: Essential oil from *Vitex negundo* is known to have repellent and insecticidal properties toward the *Anopheles gambiae* and this is linked to its monoterpene and sesquiterpene content. In this work, an effort is made to delineate the constitution of *V. negundo* essential oil (VNEO) and their interaction with odorant-binding proteins (OBPs) of *A. gambiae* and hence access its repellent efficiency as cost-effective and safer malaria vector control alternatives. (2) Methods: Anopheles species authentication was performed by genomic DNA analysis and was subjected to behavioral analysis. GC-MS profiling was used to identify individual components of VNEO. Anopheles OBPs were obtained from the RCSB protein data bank and used for docking studies. Determination of ligand efficiency metrics and QSAR studies were performed using Hyper Chem Professional 8.0.3, and molecular dynamics simulations were performed using the Desmond module. (3) Results: GC-MS analysis of VNEO showed 28 compounds (monoterpenes, 80.16%; sesquiterpenes, 7.63%; and unknown constituents, 10.88%). The ligand efficiency metrics of all four ligands against the OBP 7 were within acceptable ranges. β-selinene (−12.2 kcal/mol), β-caryophellene (−9.5 kcal/mol), sulcatone (−10.9 kcal/mol), and α-ylangene (−9.3 kcal/mol) showed the strongest binding affinities for the target proteins. The most stable hydrophobic interactions were observed between β-selinene (Phe111 and Phe120), Sulcatone (Phe54 and Phe120), and α-ylangene (Phe111), while only sulcatone (Tyr49) presented H-bond interactions in the simulated environment. (4) Conclusions: Sulcatone and β-caryophyllene presented the best log *p* values, 6.45 and 5.20, respectively. These lead phytocompounds can be used in their purest as repellent supplement or as a natural anti-mosquito agent in product formulations.

Keywords: repellent; β-caryophellene; β-selinene; sulcatone; α-ylangene; molecular docking studies; odorant-binding proteins; mosquito repellent

check for updates

Citation: Okoli, B.J.; Eltayb, W.A.; Gyebi, G.A.; Ghanam, A.R.; Ladan, Z.; Oguegbulu, J.C.; Abdalla, M. In Silico Study and Excito-Repellent Activity of *Vitex negundo* L. Essential Oil against *Anopheles gambiae*. *Appl. Sci.* **2022**, *12*, 7500. https://doi.org/10.3390/app12157500

Academic Editors: Ana Carolina Gonçalves and Andreia Filipa Silvestre Duarte

Received: 3 June 2022
Accepted: 29 June 2022
Published: 26 July 2022

Publisher's Note: MDPI stays neutral with regard to jurisdictional claims in published maps and institutional affiliations.

1. Introduction

In hot and humid regions of the world, malaria is a huge health burden. It is an acute fever sickness caused by Plasmodium parasites that are transmitted to humans by the bites of infected mosquitoes [1]. Seven mosquito species from the genus Anopheles,

which are identical morphologically speaking, act as vectors of the parasite. Six of these are behaviorally and genetically distinct [2].

Of the five malaria-causing plasmodium species (*Plasmodium vivax*, *Plasmodium ovale*, *Plasmodium malariae*, *Plasmodium falciparum*, and *Plasmodium knowlesi*), *P. vivax* and *P. falciparum* pose the most health threat with *P. falciparum* being the most widespread in Africa and *P. vivax* the most widespread in other parts of the world [3].

In the last several decades, the prevalence and incidence of malaria have grown dramatically. Malaria kills between one and two million people globally each year, with the most affected groups being pregnant women and children under the age of five [4]. According to the most recent data on the impact of disruptions to malaria prevention, diagnosis, and treatment during the COVID-19 pandemic, the worst-case scenario of a doubling of malaria mortality did not occur. However, substantial interruptions in malaria services in the year 2020 resulted in a significant rise in cases and fatalities when compared to 2019 [5].

Although surveillance data in Africa has been limited, convincing evidence of previous *P. falciparum* infections has been found in some Sub-Saharan African countries, with Nigeria (31.9%), DR Congo (13.2%), Tanzania (4.1%), and Mozambique (3.8%) accounting for more than 50% of all malaria-related deaths worldwide [6]. Given these startling statistics, it is crucial that intervention efforts and strategies be expanded.

Malaria is preventable and treatable and is, fortunately, one of the endemic illnesses for which the RTS, S/AS01 vaccination is recommended, with the vaccine greatly lowering the risk of malaria and lethal severe malaria in children [7]. Furthermore, targeting a parasite's vectors is a common and excellent method of parasitic disease management. The two primary malaria prevention approaches are the use of insecticide-treated nets (ITNs) and indoor residual spraying (IRS). Preventive chemotherapy is the use of medications, either alone or in combination, to prevent infections and their sequelae [8]. Such preventive strategies include chemoprophylaxis, intermittent preventive therapy (IPTi and IPTp) for pregnant women and children, mass medicine administration (MDA), and seasonal malaria chemoprevention (SMC) [9]. These cost-effective options complement current efforts, such as early malaria diagnosis, vector control, and treatment of confirmed cases. Consequently, increased access to WHO-recommended prevention strategies, such as effective vector control and chemoprophylaxis, has had a substantial impact on reducing the global incidence of malaria in the last two decades [10].

Today, however, mosquito resistance to pesticides is jeopardizing global efforts to control malaria [11]. Seventy-eight countries have reported resistance of the anopheles species to one or more of the four major classes of pesticides over the period 2010 to 2019, according to World Health Organization [12]. Furthermore, complete mosquito resistance to all major pesticide classes has been reported in 29 different countries [13,14]. Hence, antimalarial drug resistance in Sub-Saharan Africa over the past decade and emerging reports of drug-resistant strains are a major concern for the World Health Organization [15].

It is therefore critical to develop and define more effective and safer mosquitocidal agents with distinct modes of action. A reasonable approach to developing bio-rational vector control agents or management systems is to target or block the normal operation of mosquito endocrine systems [16]. Tremendous progress has been made in this regard, facilitating the understanding of mosquito behavior and olfactory receptors. According to Wheelwright et al. [17], specific smell-based traps and mosquito repellents can be developed by studying their olfactory systems. Olfactory receptor expression in adult mosquitoes has been found in the antennae, maxillary palps, and proboscis. This suggests that these three are peripheral olfactory organs. The three main types of receptors implicated in mosquito olfaction are gustatory receptors (GRs), odorant receptors (OR), and ionotropic receptors (IRs). ORs and IRs can detect a wide range of odorants, whereas GRs can only detect CO_2 and other volatile odorants through a heterotrimeric complex in *Anopheles* sp. Odorant [17].

The ability of mosquitoes to detect an odorant is not dependent on receptors expressed in the olfactory sensory neurons alone but also on perireceptor environment accessory pro-

teins [17]. Odorant-binding proteins (OBPs) are water-soluble, small extracellular proteins (15–17 kDa) found in the sensillum lymph of the insect sensilla [18]. They are thought to bind the odorant molecule and transport it to the receptors on chemosensory neurons via the aqueous sensillar lymph. OBPs, which are often expressed outside the chemosensory organs, are responsible exclusively as carriers of chemicals that, once solubilized, were transported to the olfactory receptors [19,20]. While it is undeniable that OBPs can bind odorants, their mechanism of interaction with odorant compounds is less clear [21]. OBP 1, 7, and 4 are members of the odorant-binding protein family and orthologs involved in host recognition signals and repellent alarm pheromones in *Aedes aegypti* [22]. OBPs are known targets for plant-based anti-mosquito insecticides [23]. One of those plants is *Vitex negundo* L. (Verbenaceae), which has been established to have repellent, insecticidal, and mosquitocidal properties linked strongly to the monoterpenes and sesquiterpenes in its content [24,25]. Progress in the identification of new targets (particularly in mosquitoes) for insecticides has been hampered over the past decade by a lack of comprehensive data on OBP mechanisms of action [26]. However, due to recent developments, availability of more current data, and scientific proofs, the structural data of key proteins implicated in OBPs action pathways may now be accessed and used.

Computer-aided molecular design is a rational strategy that combines a variety of theoretical and computational approaches routinely used in current drug research [27]. It has evolved into a powerful technique for lead screening, lead optimization, and the development of novel drug molecules, including repellant compounds [28,29]. When compared to traditional experimental approaches, the aim is to speed up the process while simultaneously lowering cost and allowing for the capacity to deal with big, diversified databases of ligands. The goal of this study is to evaluate the potential of anopheles mosquito OBPs as targets for *V. negundo*-based anti-mosquito repellent molecules in silico and in vitro using X-ray crystallographic structural data of mosquito OBPs in the complex.

2. Materials and Methods

2.1. Collection and Identification of V. negundo Leaves

In August 2021, the leaves of *V. negundo* were harvested in Benue State, Nigeria. The leaves were identified, and voucher specimen number NARICT/BSH/1610 was deposited at the National Research Institute for Chemical Technology (NARICT) in Zaria, Nigeria.

2.2. Leave Handling and Extraction

Fresh leaves of *V. negundo* were collected, washed, and extracted separately within 12 h of collection. Extraction was performed according to the procedure of Okoli et al. [30] with a 25 kg capacity fabricated essential oil distillation system (EDS). The plant was extracted for 45 min, and the distillates were recovered and separated into essential oil and hydrosol using a 2 L separatory funnel. The essential oil was then dried over anhydrous Na_2SO_4 before being stored for further analysis.

2.3. GC-MS Profiling of the Essential Oils

GC-MS analysis of *V. negundo* essential oil was performed using a Varian CP3800 gas chromatograph with an HP5 capillary column (30 mm 0.25 mm, thickness 0.25 m), a flow rate of 1.2 mL/min, and gas carrier ion nitrogen grains. Varian Saturn 2000 Trap Detector Temperatures in the oven were gradually increased from 50 to 280 °C at a rate of 3 °C/min. Analysis conditions: injection temperature and transmission line temperatures of 220 and 240 °C, respectively. Injection volume: 0.2 L of 10% hexane solution, 1:30 ratio. The co-production of essential oils with solutions comprising C8-C22 alkanes of the same class results in a precise maintenance index for all molecules. Individual components are identified using storage indicators, which are then compared to previously described chemicals in the literature [31,32]. In addition, a computer library linked to GC-MS (Wiley 275L), Adams Library [https://bok.cc/book/3506611/3b1f4f] (accessed on 3 March 2022), NIST website [https://webbook.nist.gov/chemistry/] (accessed on 5 March 2022). Use

comparable white columns and/or RI values from the Mondello library [https://www.sisweb.com/software/wileyffnsc.htm] (accessed on 3 March 2022).

2.4. Preparation of Targets

Uniprot (http://www.uniprot.org/) (accessed on 11 May 2022) was used to compile all of the protein information. OBP 1 (PDB ID 3N7H), OBP 7 (PDB ID 3R1O), OBP 4 (PDB ID 3Q8I), and OBP 5 (PDB ID 3Q8I) are four *A. gambiae* OBP targets that were retrieved from the RCSB protein data bank (http://www.rcsb.org) (accessed on 11 May 2022) (PDB ID 2ERB). To view the protein and eliminate all water molecules from the structure, we used the PYMOL (version 1.7.4.5 program, Madison, WI, USA). The Swiss PDB (viewer v4.1.0, Basel, Switzerland) was used to repair void atomic spaces and crystallographic disturbances using energy reduction. The ".pdb" format was used to preserve the improved protein structure.

2.5. Ligands Preparation

In this study, all phytocompounds identified from the GC-MS analysis in the essential oils were retrieved from the PubChem database (www.pubchem.ncbi.nlm.nih.gov) (accessed on 21 March 2022) and saved in the Structure Data Format (SDF). Further, N,N-diethyl-3-methylbenzamide (DEET) (PubChem CID 4284) was selected as a positive control because it is widely used as a chemical repellent against a variety of insects [33,34], strong electrophysiological responses [35], and interference with the olfactory receptor neurons/receptors resulting in avoidance behavior [36].

2.6. QSAR Studies

The physico-chemical properties of the FLP in correlation to biological activity were studied using QSAR modeling on the Hyper Chem (Professional 8.0.3 program, New Delh, India). The structure of each of the FLP was optimized with a semi-empirical PM3 method using a (MM+) force field, while a Fletcher-Reeves conjugate gradient algorithm was used for the energy minimization. A range of QSAR parameters, including hydration energy, free energy, refractivity, total energy, surface area, polarizability, volume, dipole moment, RMS gradient, mass, and partition coefficient (log P), were calculated.

2.7. Molecular Docking and Binding Site Prediction

In silico molecular docking with the aid of AutoDock vina (version 4; The Scripps Research Institute, La Jolla, CA, USA) was used to find the suitable binding orientations and conformations of the ligand with the targeted proteins. This is necessary for calculating the ligand′s preferred orientations with the highest binding affinities for the protein′s active sites, which are connected with structural pockets and cavities. The drug′s binding to specific amino acid residues was displayed in the BIOVIA Discovery Studio visualizer (v16.1.0.15350, Paris, France) after molecular docking.

2.8. Molecular Dynamics Simulation

The stability of the lead phytochemicals from the docking analysis complexed with the odorant-binding protein 7 was observed over 100 ns molecular dynamics simulation MDS studies using the Desmond module of Schrodinger 2019-4 in the explicit solvent system with an OPLS3 force field.

A 10 Å buffer region of orthorhombic periodic boundary conditions was used with a solvated system of TIP3P molecules. The system was subsequently neutralized by counter ions (Na+) in an ensemble (NPT) of Nose-Hoover thermostats with a barostat to maintain a consistent temperature (310 K) and constant pressure (1 bar) for all the systems [37]. The hybrid energy minimization strategy, which was followed by conjugate gradient techniques, was created with the steepest descent of over 1000 steps. For energy reduction, the Broyden-Fletcher-Goldfarb-Shanno (LBFGS) method with a convergence threshold gradient of 1 Kcal/mol/Å was also used.

The smooth particle mesh Ewald technique was used to calculate electrostatic interactions within a cut-off radius of 9 Å for short-range van der Waals and Coulomb interactions. The reference system propagator algorithms (RESPA) integration for multiple time steps was used in the dynamics study of bonded (2 fs), near (2 fs), and far-bonded (6 fs) interactions. The data were collected for every 100 ps, and the obtained trajectory was analyzed with Maestro graphical interphase. Various structural and thermodynamic parameters were computed from the trajectory files of the individual systems.

2.9. Rearing, Identification, Genomic DNA Extraction, and PCR Amplification of Anopheles Species

Collection of mosquito larvae was performed from a 0.12 m × 2.5 m deep temporary pool with grass vegetation in Kaduna State, Nigeria, and identification of larvae was performed at the sites of breeding, along with morphological classification. The larvae were then transported to the Biological Sciences laboratory insectary of Kaduna State University, Nigeria. They were then sorted into the Anophelinae subfamilies using the Coetzee, [38] identification key under a compound microscope. After a 2 h acclimatization period, the immature larvae were fed a low-fat flour-baked product and then transferred to breeding chambers. There, they were reared to adulthood in a separate square wooden chamber for three weeks at 25 °C, 65% relative humidity, and a regulated light-dark (14/10 h) cycle.

Using a basic Olympus light microscope, the emerged adults were identified morphologically using taxonomic characters such as palps, proboscis, wing venation, markings, or tuffs on legs or abdomen as provided by the dichotomous keys used by Coetzee [38]. The adults in the cages were fed a 10% sucrose solution after eclosion from their pupal cases and allowed to rest and grow for 2 to 3 days. Only newly emerged adult female *A. gambiae* were manually aspirated into a 200 mL perforated plastic container and allowed to rest for one hour before being exposed to the essential oil mixture and pure components (Figure 1).

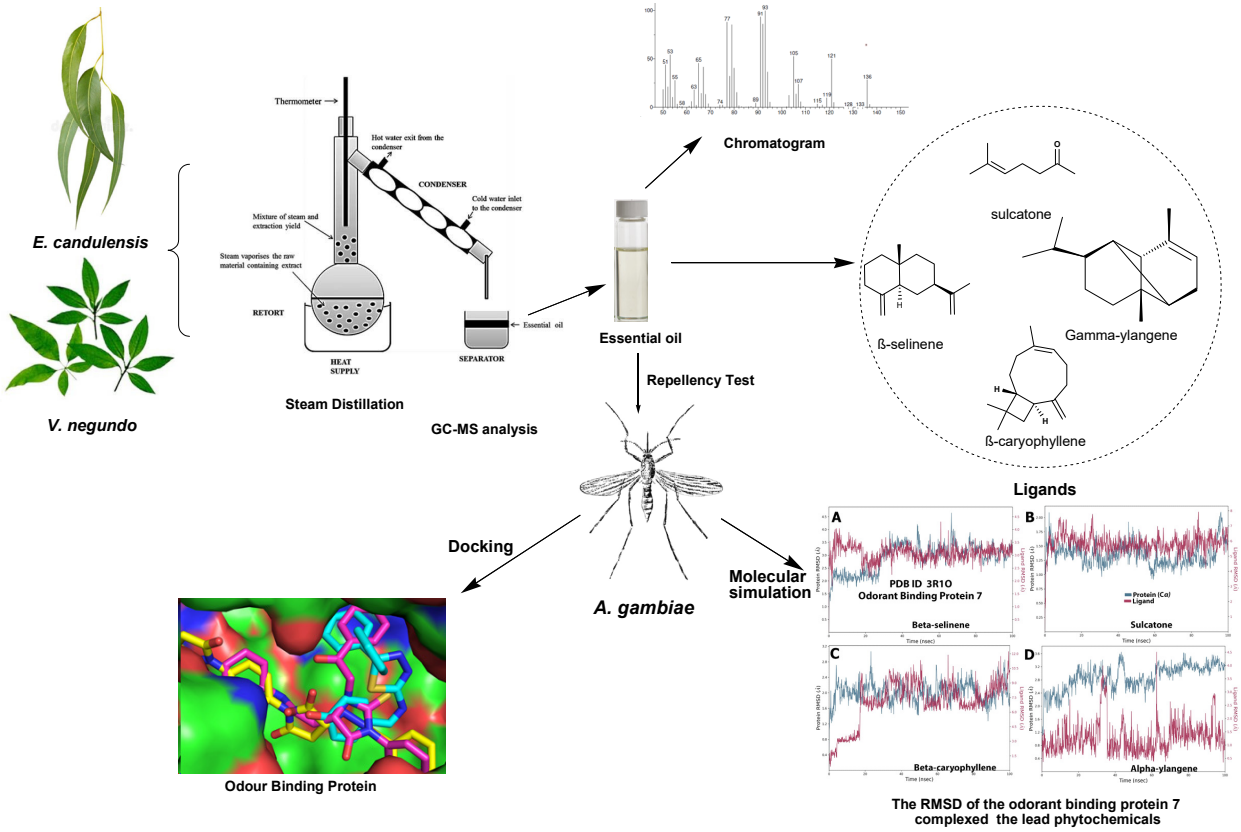

Figure 1. Graphical illustration of repellency and odorant-binding protein efficiency using a molecular docking-based technique. (**A**) β-Selinene, (**B**) Sulcatone, (**C**) β-caryophyllene, and (**D**) α-ylangene.

Genomic DNA (gDNA) was extracted from 20 adult Anopheles mosquitoes using the Quick-DNATM Miniprep Plus Kit (D4069) product by ZYMO Research Company according to the manufacturer's protocol, as described by Okoli et al. [30]. Adult mosquitoes from the *Aedes gambiae* (s.l) complex were tested using PCR and genomic DNA assays for species identification, molecular form identification, and molecular analysis. Ahmadu Bello University, Zaria, Nigeria, conducted the molecular analyses.

2.10. Mosquito Behavioral Study

The mosquito behavioral responses to the *V. negundo* essential oil were conducted at an optimal repellency concentration of 0.48% v/v, determined in a previous study by Okoli et al. [30]; while the pure constituents (analytical purity, Sigma-Aldrich (Johannesburg, South Africa) were selected based on their binding energies. A 1.5 g cotton ball was immersed into the solution of essential oil and selected compounds in petrolatum, which was then mounted on the cotton ball holder of the test arm of the olfactometer [39]. Pure petrolatum was used as a negative control, and the air stream within the chamber was controlled at a rate of 180 mL/min using an electric air pump.

Behavioral responses were monitored and recorded for 1 h in a glass olfactometer containing precisely 150 female *A. gambiae* mosquitoes [40]. The olfactometer was air cleaned with a stream of hot air (>60 °C) after each investigation, and the cotton ball was removed, and the holder cleaned. The olfactory test was carried out three times. The repellent rate was calculated using the equation below (1) [41]:

$$\% \text{ Repelled } = 100 - \left(\frac{\text{mean number of mosquitoes selecting essential oil/pure compound}}{100 - \text{ mean number of mosquitoes not selecting essential oil/pure compound}} \right) 100 \quad (1)$$

The Probit analysis model in IBM SPSS v.25 statistical software (Chicago, IL, USA) was used to estimate the 50% mosquito repelled rate.

3. Results and Discussion

3.1. PCR Confirmation of Anopheles Gambiae s.s

The PCR amplicons examined under the trans-illuminator UV light revealed positive bandwidths of 390 bp for *A. gambiae* and 315 bp for *A. arabiensis* (Plate S1). Positive bandwidths of 390 bp were seen in the PCR amplicons when seen under the trans-illuminator UV light. After conditioning the PCR, samples 1–7 of randomly selected *A. gambiae* s.l displayed DNA bandwidths of 475 bp, confirming the species to be *A. gambiae* s.s (Plate S2).

3.2. Chemical Composition of V. negundo Essential Oils

Table 1 shows the results of the *V. negundo* essential oils GC-MS analysis, and the chromatograms are presented in Figure S1. The essential oil contained 28 known compounds. Monoterpene and sesquiterpene contents are 80.16% and 7.63%, respectively, while other unknown constitutes account for about 10.88%. The observed compounds are in consonance with the reports of Gill et al. [42] and Huang et al. [43].

The major components are α-pinene (27.94%), myrcene (16.78%), sabinene (8.38%), and cis-linalool oxide (6.72%), and borneol (5.20%), as well as (E)-β-ocimene (0.65%), trans-linalool oxide (0.88%), n-decanal (0.67%), α-cubebene (0.65%), β-bourbonene (0.94%), β-elemene (0.67%), α-gurjunene (0.77%), β-caryophyllene (0.64%), trans α bergamotene (0.68%), β-selinene (0.82%), and ledene (0.67%). Some monoterpenes and sesquiterpenes such as α-pinene, myrcene, linalool, α-terpinolene, and citronellal with reported potent insecticidal properties were present in the oils [44–46].

3.3. Molecular Docking

The binding energies of the GC-MS-identified phytocompounds from essential oils of *V. negundo* to four *A. gambiae* OBPs proteins are reported in Table S1. Four phytocompounds that demonstrated a multiplicity of binding properties to the four proteins with varying degrees of interaction within the active pockets of the proteins were selected as the lead phy-

tocompounds. In Table S1, β-caryophellene (−9.5 kcal/mol), β-selinene (−12.2 kcal/mol), sulcatone (−10.9 kcal/mol), and α-ylangene (−9.3 kcal/mol) demonstrated the lowest binding energy for OBP7 compared to OBP1, OBP4, and OBP.

Table 1. Compositional variation in the essential oils of *V. negundo*.

RT	%	Compounds	RI_{Exp}	RI_{Lit}
5.750	27.94	α-pinene	934	931
7.271	1.28	sulcatone	965	960
7.800	8.38	sabinene	983	975
8.289	16.78	myrcene	994	993
8.384	1.44	α 3-carene	1012	1010
8.805	0.65	(E)-β-ocimene	1032	1029
9.192	6.72	Cis-linalool oxide	1088	1086
9.633	0.88	trans-linalool oxide	1098	1092
9.776	1.16	linalool	1105	1102
9.871	1.03	cis-sabinene hydrate	1178	1174
10.76	1.81	camphor	1318	1316
11.01	2.06	citronellal	1395	1389
11.61	5.20	borneol	1414	1409
11.96	1.05	α-terpineol	1445	1437
12.07	1.52	verbenone	1456	1452
12.52	0.67	n-decanal	1459	1454
12.61	2.87	geraniol	1491	1489
13.01	3.95	linalyl acetate	1494	1492
13.47	1.94	bornyl acetate	1499	1498
13.86	3.71	4-terpinenyl acetate	1526	1522
14.62	0.65	α-cubebene	1561	1561
14.93	0.97	α-ylangene	1574	1574
15.56	0.82	α-copaene	1578	1576
15.99	0.94	β-bourbonene	1589	1582
16.14	0.67	β-elemene	1599	1592
16.56	0.77	α-gurjunene	1610	1608
16.68	0.64	β-caryophyllene	1637	1638
17.10	0.68	trans α bergamotene	1643	1649
18.12	0.82	β-selinene	1889	1889
18.59	0.67	ledene	1891	1890
	1.33	Unknown		
Monoterpenes	80.16			
Sesquiterpenes	7.63			
Others	10.88			

RT: retention time (min), RI_{Exp}: experimental retention index, and RI_{Lit}: literature retention index [31,43,47].

β-selinene had the highest binding energies (−11.1, −11.2, and −12.2 Kcla/mol) to three of the OBPs (OBP 1, OBP 4, and OBP, respectively), thereby exhibiting a multiplicity of binding tendencies. β-selinene, in part or in association with the four lead phytochemicals, may be involved in the functional blocking of the olfactory receptor co-receptors, which underlines the activities reported. The four lead phytocompounds from the docking studies were selected for further computational investigation.

3.4. Amino Acid Interaction of Lead Phytocompounds with Selected A. gambiae OBP

The four lead phytocompounds demonstrated the highest binding energy to the OBP 7 (3R1O) than the other 3 OBPs; hence, it was selected for further interactive analysis with

the lead phytocompounds. The interaction of the FLP with amino acid residues of the binding pocket of OBP 7 (3R1O) is presented in Table 2.

Table 2. Amino acid interaction of lead phytocompounds with *A. gambiae* OBP 7 (3R1O).

S/No	Compounds	Binding Energy (Kcal)	Interacting Amino Acid Residues
1	Beta-selinene	−12.2	Phe54, Phe111,Pro41, Tyr49, Phe120
2	Sulcatone	−10.9	Phe54, Phe111, Phe120, Pro13, Tyr49
3	Beta-caryophyllene	−9.5	Phe54, Phe111, Phe120, Pro41
4	Alpha-ylangene	−9.3	Phe54, Phe111, Phe120, Pro41, Tyr49

It was observed that all FLP interacted with amino acid residues Phe54, Phe111, Phe120, and Pro41 majorly through hydrophobic interactions (Figure 2).

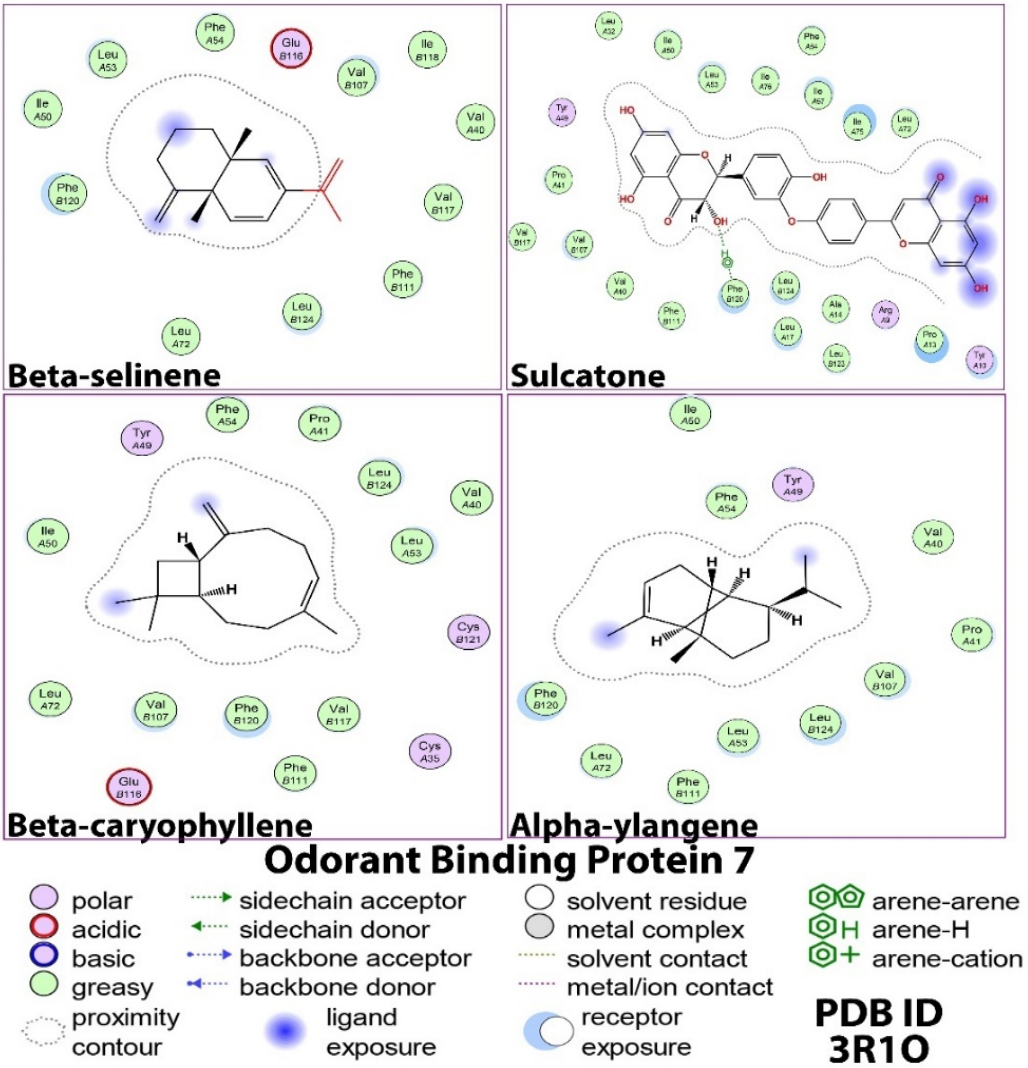

Figure 2. Two-dimensional representation of post-docking interactions of the lead phytocompounds with *A. gambiae* OBP 7.

Previous experimental binding studies have established that the binding grooves of the *A. gambiae* OBPs are elongated hydrophobic groves that are capable of accommodating both linear and polycyclic compounds. The FLP interacted with binding site residues of known inhibitory compounds, including the AZO and palmitic acid binding sites. The properties of the interacting residues were responsible for the multiple hydrophobic interactions. It

was also observed that the FLP exhibited a similar orientation in the hydrophobic pocket of the selected *A. gambiae* OBP. Though the pocket is elongated, the FLP is accommodated in the same region of the binding pocket (Figure 3).

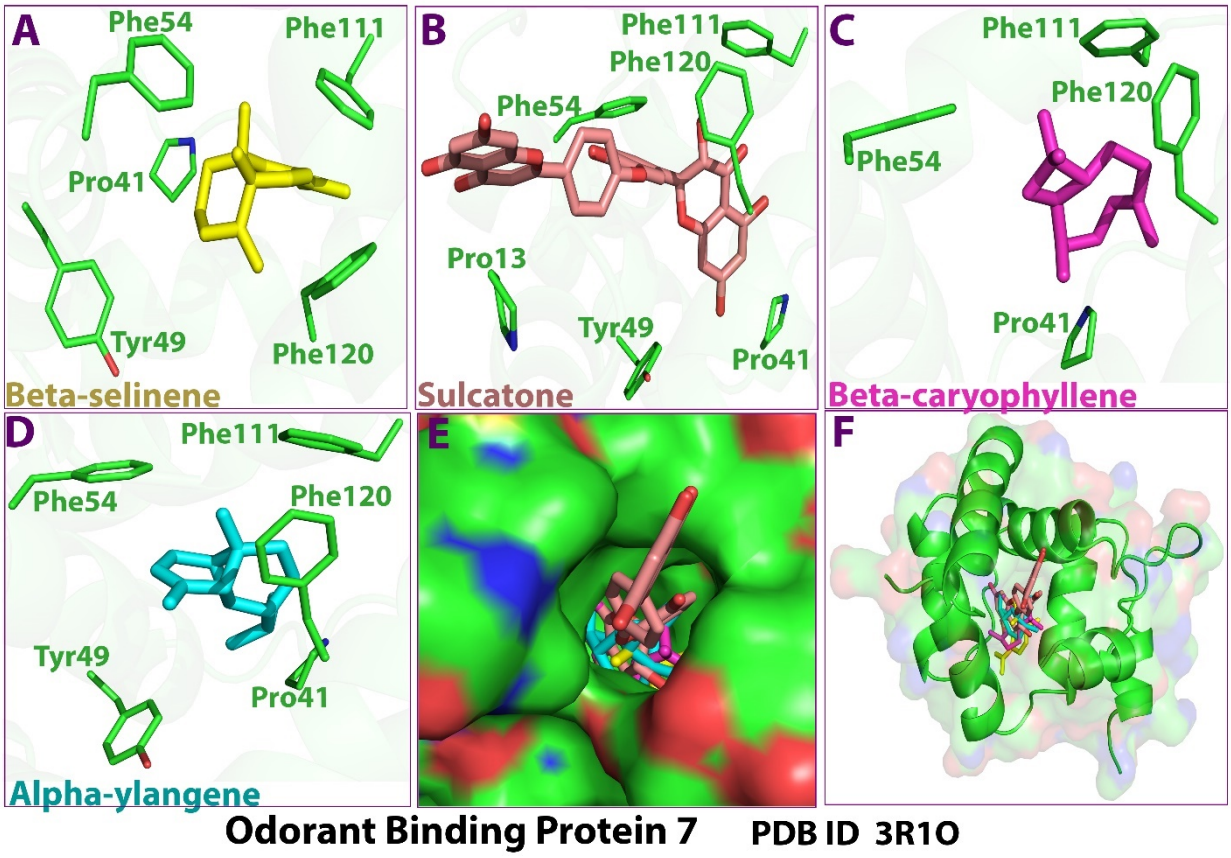

Figure 3. Three-dimensional representation of post-docking interactions of (**A**) β-Selinene, (**B**) Sulcatone, (**C**) β-caryophyllene, (**D**) α-ylangene (**E**) all lead phytochemical in the active pocket, and (**F**) 3D orientation of all lead phytochemical with *A. gambiae* OBP 7.

3.5. Efficiency Metrics of Four Ligands

Table 3 shows the ligand efficiency metrics of the selected ligands. Ligand efficiency (LE), ligand lipophilic efficiency (LLE), and fit quality (FQ) are expected to have threshold values of 0.3, 3, and 0.8 for a molecule to be classified as a potential hit quantitatively [48]. During lead discovery, the ligand efficiency lipophilic price (LELP) is estimated to be between −10 and 10 [49]. The ligand efficiency metrics of the four ligands against the OBP are within the criteria, qualifying them as a possible odorant-binding protein repellent compound.

Table 3. Ligand efficiency metrics.

Compounds	LE	LE_{scale}	LLE	FQ	LELP
Sulcatone	1.2111	0.6269	7.6746	1.9320	0.2876
α-ylangene	0.6213	0.5271	6.3137	1.1763	0.8572
β-caryophyllene	0.6333	0.5271	6.4752	1.2016	0.8166
β-selinene	0.8133	0.5271	8.4638	1.5431	0.6343

3.6. QSAR Studies

The physico-chemical properties of the FLP in correlation to biological activity as computed from their QSAR parameters are presented in Table 4.

Table 4. Physico-chemical properties of the FLP computed from their QSAR parameters.

Function	Beta-Selinene	Sulcatone	Beta-Caryophyllene	Alpha-Ylangene
Surface Area (Approx) (Å^2)	377.12	854.51	316.37	244.90
Surface Area (Grid) (Å^2)	436.07	789.53	383.68	386.42
Volume (Å^3)	746.45	1357	626.27	612.24
Hydration Energy (Kcal/mole)	1.02	−38.48	−0.04	−0.10
Log P	5.20	6.45	0.77	0.47
Refractivity (Å^3)	41.81	73.79	28.31	19.75
Polarizability (Å^3)	27.82	48.93	14.17	14.31
Mass (amu)	214.35	542.37	180.17	180.17
Total Energy (kcal/mol)	18.4378	15.5186	53.0244	96.0766
Dipole Moment (Debye)	0	0.5526	0	0
RMS Gradient (kcal/Å mol)	0.08942	0.09325	0.0975	0.09742

Sulcatone and beta-selinene presented the best QSAR parameters. For instance, both compounds exhibited the highest partition coefficient log *p*-value, which is important in evaluating the rate of permeability into cell membranes [50].

3.7. Frontier Molecular Orbitals (FMO) Studies

The chemical reactivity and the most likely reactive sites of the FLP were studied using FMO analysis (Figure 4).

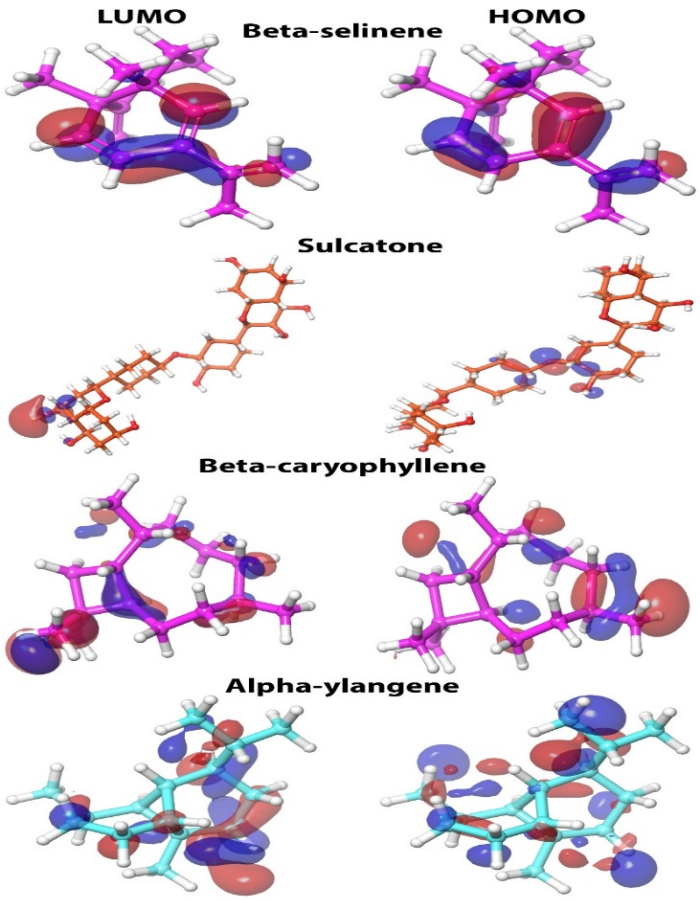

Figure 4. Optimized structures of the four lead phytocompounds from the docking studies using FMOs.

The calculated energies, EHOMO and ELUMO, of compounds help to explain the global reactivity descriptors such as chemical potential, chemical hardness, and electrophilicity of the FLP were elucidated from the computed EHOMO and ELUMO, while the negative values obtained for the EHOMO and ELUMO were confirmatory of the stability of the FLP. It was observed that β-caryophyllene had the least band energy gap (EHOMO-ELUMO) compared to other phytocompounds. Therefore, β-caryophyllene demonstrated the highest chemical reactivity. The parameters that measure the chemical reactivity of the FLP, such as chemical potential (μ), electronegativity (χ), global hardness (η), global electrophilicity index (ω), and global softness (S), were calculated (Table S2). Sulcatone had the least chemical softness (S) hence, predicted to have higher stability than the other FLP. The electrophilicity (χ) is another important parameter that measures the ability of a compound to accept electron(s) from its surrounding. B-caryophyllene showed less electrophilicity than other compounds.

3.8. Interpretation of Molecular Dynamic Analysis

A full all-atom 100 ns molecular dynamics simulation was performed on the complexes of the lead phytochemicals (β-selinene, β-caryophellene, sulcatone, and α-ylangene) with the odorant-binding protein 7. The obtained MD simulation trajectories for the four systems were further analyzed using different structural and thermodynamic parameters.

3.9. Ligand Properties

The lead phytochemicals were analyzed relative to the reference conformation in the protein. Various structural parameters were plotted for each of the systems, including the root mean square deviation (RMSD), radius of gyration (rGyr), intramolecular hydrogen bonds (intraHB), molecular surface area (MolSA) within 1.4 Å probe radius, solvent accessible surface area (SASA), and polar surface area (PSA) (Figures S2–S5). After equilibration at the beginning of the simulation, a stable RMSD was observed for the β-caryophellene and sulcatone systems, while minimal RMSD fluctuation (<3.0 Å) was observed for the β-selinene and α-ylangene systems, thus indicative of no immense dynamical alteration [51]. The rGyr profiles for the four systems were stable throughout the simulation period, suggesting no alterations in the chemical structure of the ligands [52]. Besides sulcatone, the three other phytochemical systems displayed no intramolecular hydrogen bond (intraHB) plots. The MolSA and SASA for the four phytochemicals in the referenced systems were in acceptable ranges, indicating that they were imposingly stable in the complexes during the simulation run.

3.10. Protein Secondary Structure

The secondary structure elements (SSE) of the odorant-binding protein 7 upon the binding of the lead phytochemicals such as alpha-helices and beta-strands were analyzed during the simulation period. Figure 5 shows the SSE distribution by residue index throughout the protein structure. The total SSE (%) for the protein upon the binding of β-selinene, β-caryophellene, sulcatone, and α-ylangene is 55.38, 54.51, 54.12, and 47.83, while the alpha-helices (%) and beta-strands (%) were, respectively, 53.35 and 2.02; 54.36 and 0.14; 53.09 and 1.03; 47.74 and 0.09 for β-selinene, β-caryophellene, sulcatone, and α-ylangene bound systems (Figure 5A–D). The analysis of the four systems shows that binding of the α-ylangene to the protein minimally reduced the SSE of the odorant protein, hence the conformational integrity of the protein (Figure 5D).

3.11. Protein Root Mean Square Fluctuation

The RMSF residual index is valuable for depicting local changes along the protein chain during the simulation. Figure 6A–D shows the RMSF plots of odorant-binding protein 7 complexed with the lead phytochemicals.

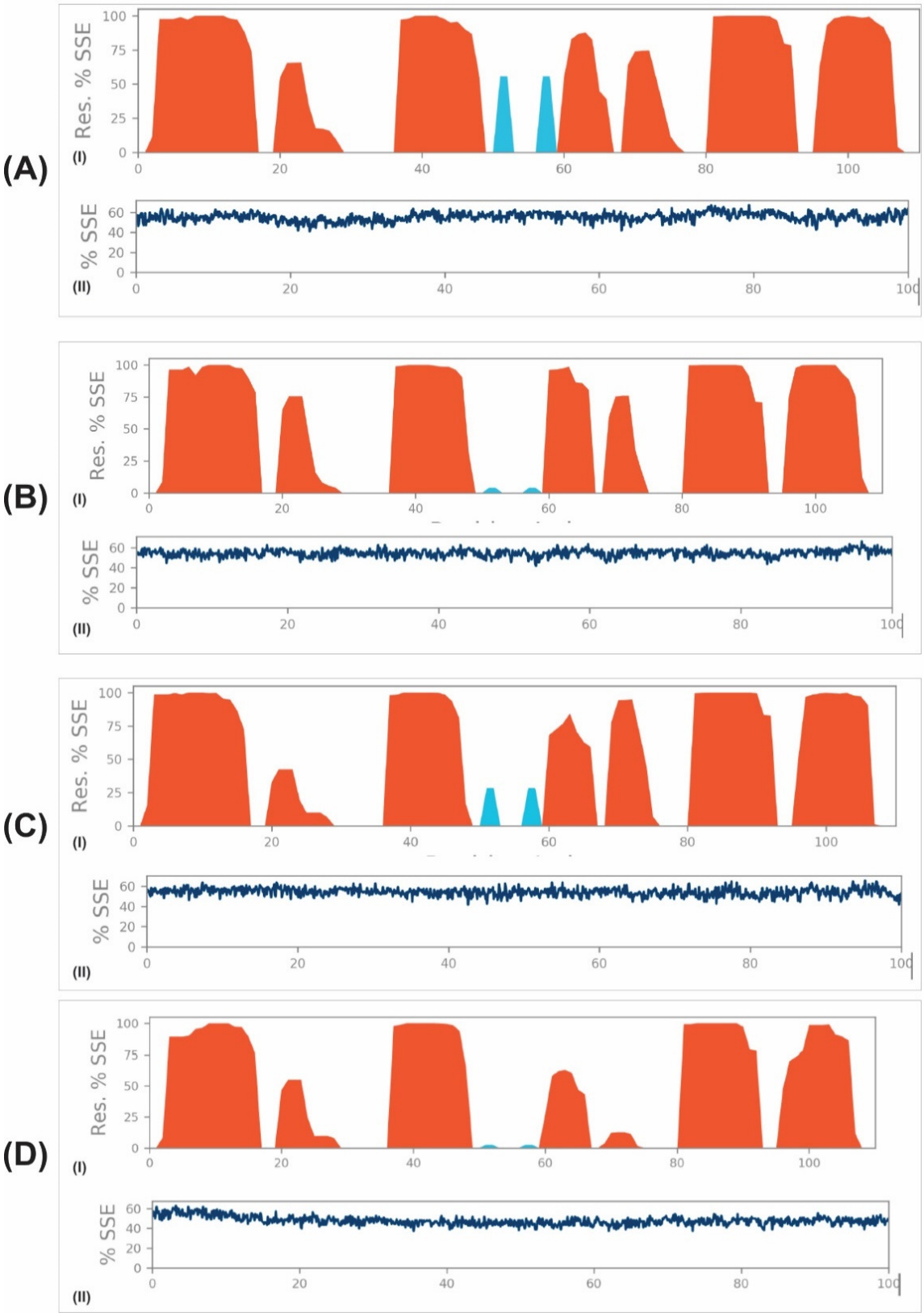

Figure 5. The secondary structural analysis of odorant-binding protein 7 during 100 ns MD simulation (aI SSE distribution by residue index throughout the protein structure (alpha-helices: red and beta-strands: blue) (II) summary of the SSE composition for each trajectory frame on interaction with (**A**) β-Selinene, (**B**) Sulcatone, (**C**) β-caryophyllene, (**D**) α-ylangene.

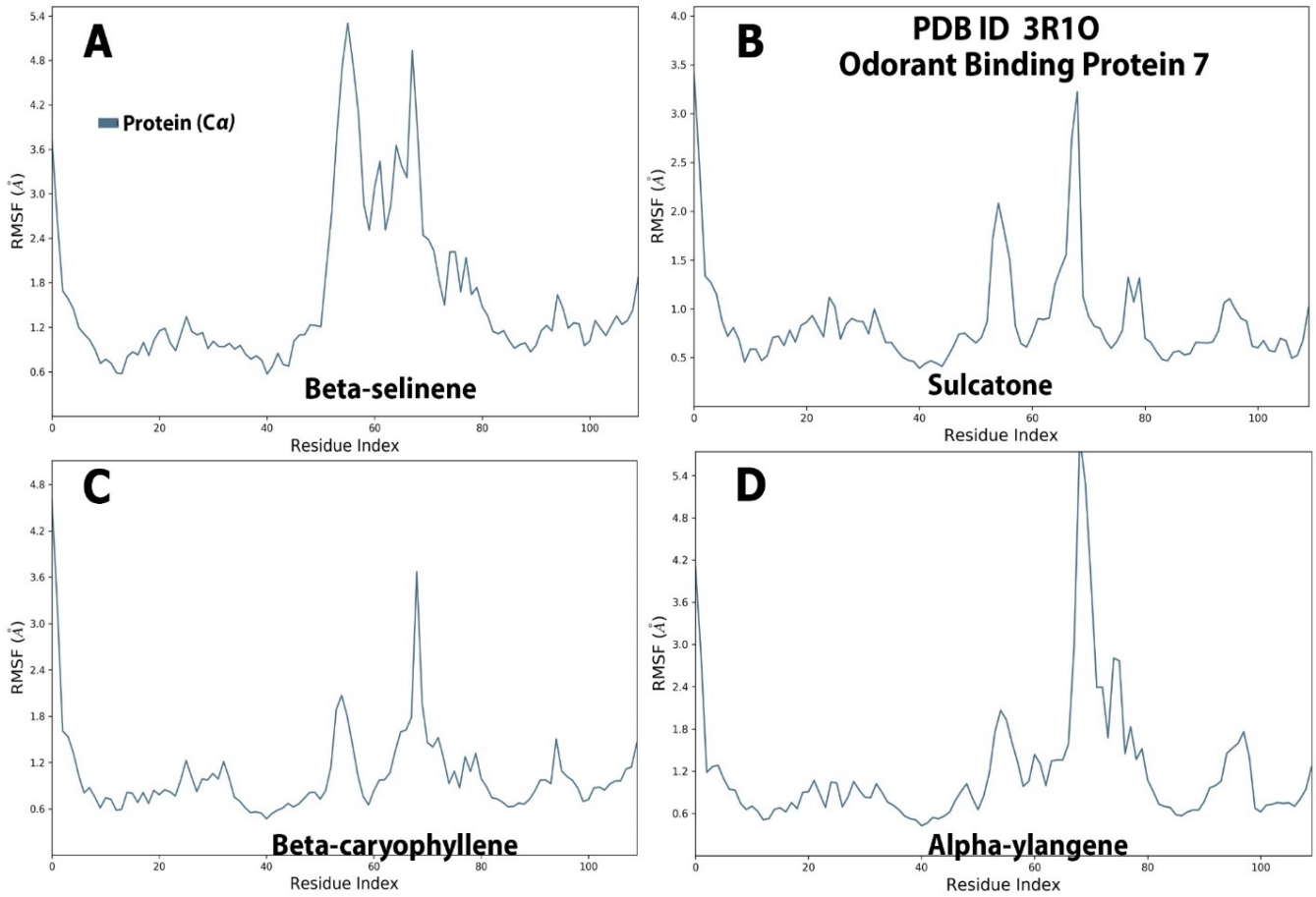

Figure 6. The root mean square fluctuation RMSF analysis of odorant-binding protein 7 complexed with the (**A**). β-Selinene, (**B**) Sulcatone, (**C**) β-caryophyllene, (**D**) α-ylangene.

The peaks indicate areas of the protein with the highest fluctuations during the course of the simulation. Besides the fluctuation at the terminals of the plots, peaks were observed between the 40 and 80 ns time frames for all four systems. This corresponds to the unstructured region of the proteins. The structured regions (alpha-helical and beta-strand) presented less fluctuation than the unstructured region (usually the loop region) of the protein. The high peaks did not necessarily reflect a compromise in the integrity of the protein structure but motion due to the absence of a structured unit at that time frame.

3.12. Protein-Ligand Contacts

The stacked bar interaction plots that are categorized by type (hydrogen bonds, hydrophobic, ionic, and water bridges) of interactions were used to study the protein-lead phytochemical interactions or contact throughout the simulation period (Figure 7). Using the distance of 2.5 Å between the donor and acceptor atoms as the geometric criteria for H-bond, only the sulcatone bound system presented several H-bond interactions in the simulated environment. Among other H-bonds, the highest H-bond interaction fraction with about 92% contact time of the whole simulation time was between sulcatone and residue Tyr49.

Sulcatone also made several salt bridges with various residues of the odorant protein. The presented hydrogen-bonded protein-ligand interactions that were mediated by water molecules in the plot were selected using the geometric criteria for a protein-water or water-ligand H-bond of 2.8 Å. Figure 7B shows that Glu116, Lys119, and Arg9 made the highest salt bridges with the ligand groups of sulcatone. Several hydrophobic contacts, including pi-cation, pi-pi, and other non-specific interactions, were observed with different residues of the odorant proteins. Among the several hydrophobic interactions, Phe111 and Phe120

of the odorant protein maintained the highest hydrophobic contact of more than 45% of the simulation time with β-selinene. Sulcatone maintained the highest hydrophobic contact with Phe54 and Phe120 for more than 40% of the simulation period. β-caryophellene presented several contacts of less than 20% of the simulation with the odorant protein, while the hydrophobic contact between α-ylangene and residue Phe111 was maintained for more than 40% of the simulation time. An in-depth analysis plot of the various types of interactions that occurred over the simulation period of 100 ns was further presented in a timeline representation in Figure 8. The top panel shows the detailed contacts the odorant protein made with the lead phytochemicals over the course of the trajectory, while the bottom panel shows the residue in contact with the ligand in each of the trajectory frames.

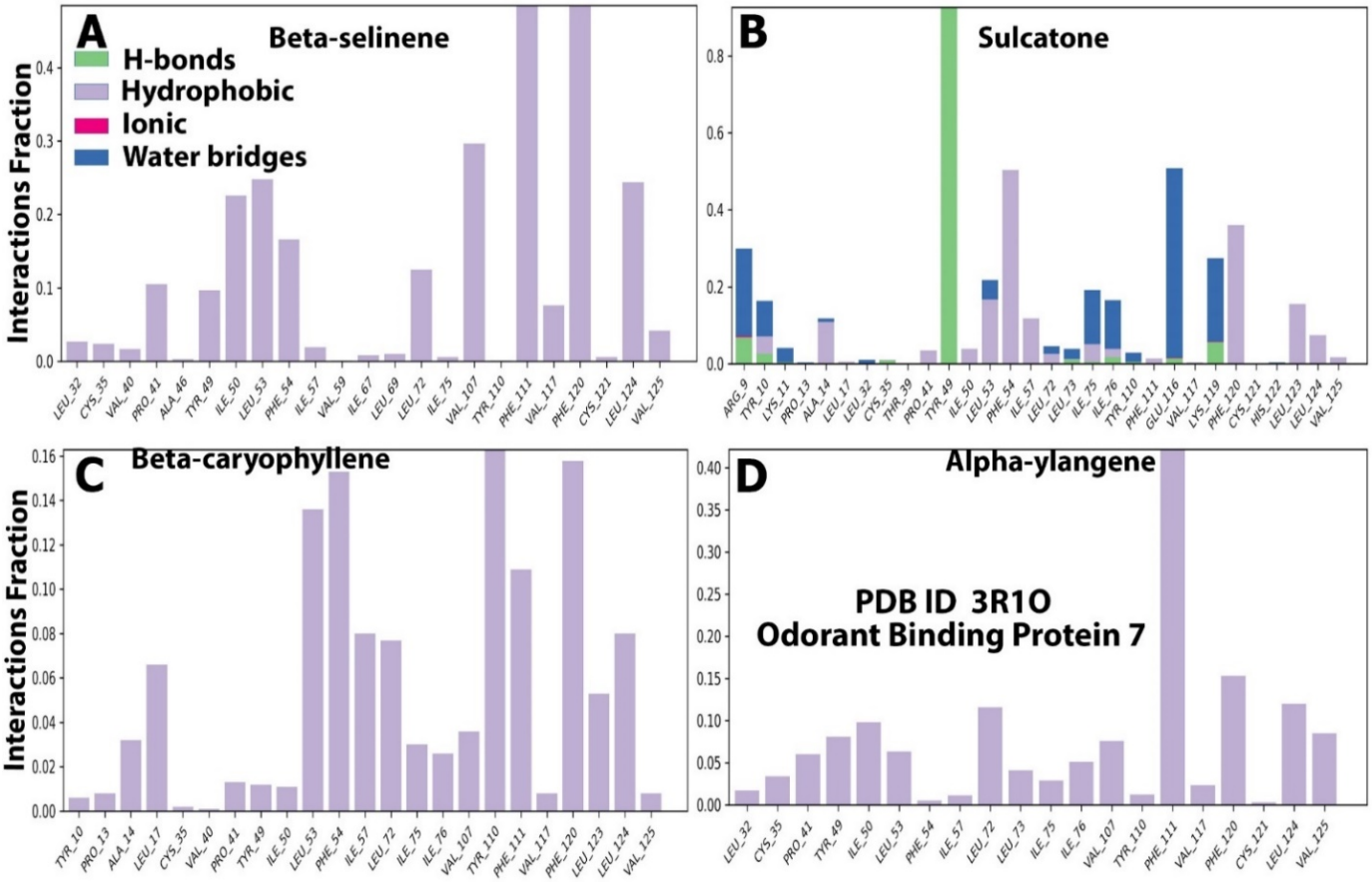

Figure 7. A stacked bar interaction plots of the residues of the odorant-binding protein 7 with the lead phytochemicals (**A**–**D**) in the selected trajectory across the MD simulation period of 100 ns.

3.13. Root Mean Square Deviation Analysis

The root mean square deviation (RMSD) measures the alteration in the displacement of atoms for a particular frame with respect to a reference frame for all the trajectories. Figure 9A–D shows the RMSD of the odorant-binding protein 7 in complex with the lead phytochemicals. The red line (left Y-axis) in the plots shows the RMSD evolution of the protein after all protein frames are first aligned on the reference frame backbone. The ligand RMSD (right Y-axis) shows how stable the lead phytochemicals are with respect to the protein. The protein-ligand complex was first aligned on the reference protein backbone. Figure 9A shows the plots of the RMSD of the β-selinene complex system.

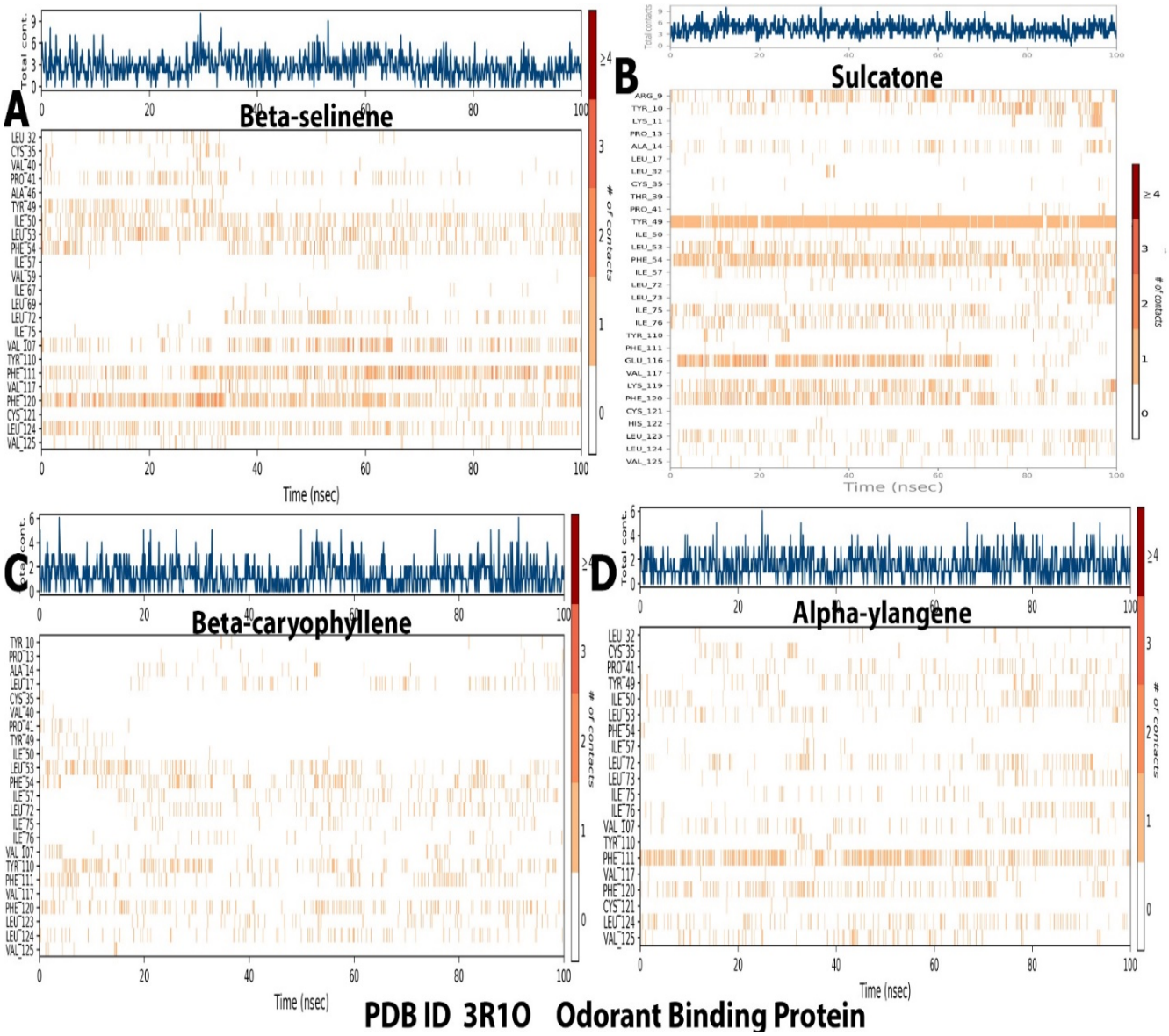

Figure 8. A timeline representation of interactions and contacts (H-bonds, hydrophobic ionic, water bridges) between the residues of the odorant-binding protein 7 and the lead phytochemicals (**A**–**D**) in the selected trajectory across the MD simulation period of 100 ns.

The protein RMSD was equilibrated before the first 10 ns, while the ligand RMSD was equilibrated after the first 20 ns. Both systems were stabilized with minimal fluctuations and converged at 100 ns. Both the protein and ligand RMSD for the sulcatone complexed system were equilibrated before 10 ns of the simulation with minimal fluctuation (less than 2 Å) after equilibration. The protein RMSD of the β-caryophellene bound system was equilibrated after 20 ns with a sharp peak after equilibration, while the ligand RMSD was equilibrated at the beginning of the simulation. Both systems experienced minimal fluctuations that were within the acceptable range of <3 Å, and convergence was also reached toward 100 ns. The protein RMSD plots for the α-ylangene bound system followed a different pattern from the ligand RMSD. Both systems experienced minimal fluctuations that were within the acceptable range of <3 Å, and convergence was also reached toward 100 ns. The protein RMSD plots for the α-ylangene bound system followed a different pattern from the ligand RMSD. Both systems were equilibrated before 20 ns but experienced several deep and peak fluctuations throughout the simulation. The deviance in the RMSD plots further explains the reduction in the secondary structure elements (alpha-helices

and beta-strands) (Figure 5D). The binding of α-ylangene reduced the stability of the protein [53]. In general, the odorant protein complexed with the lead phytochemicals except α-ylangene demonstrated a high degree of structural stability and compactness [54]; hence, the systems can be adapted for other experimental models.

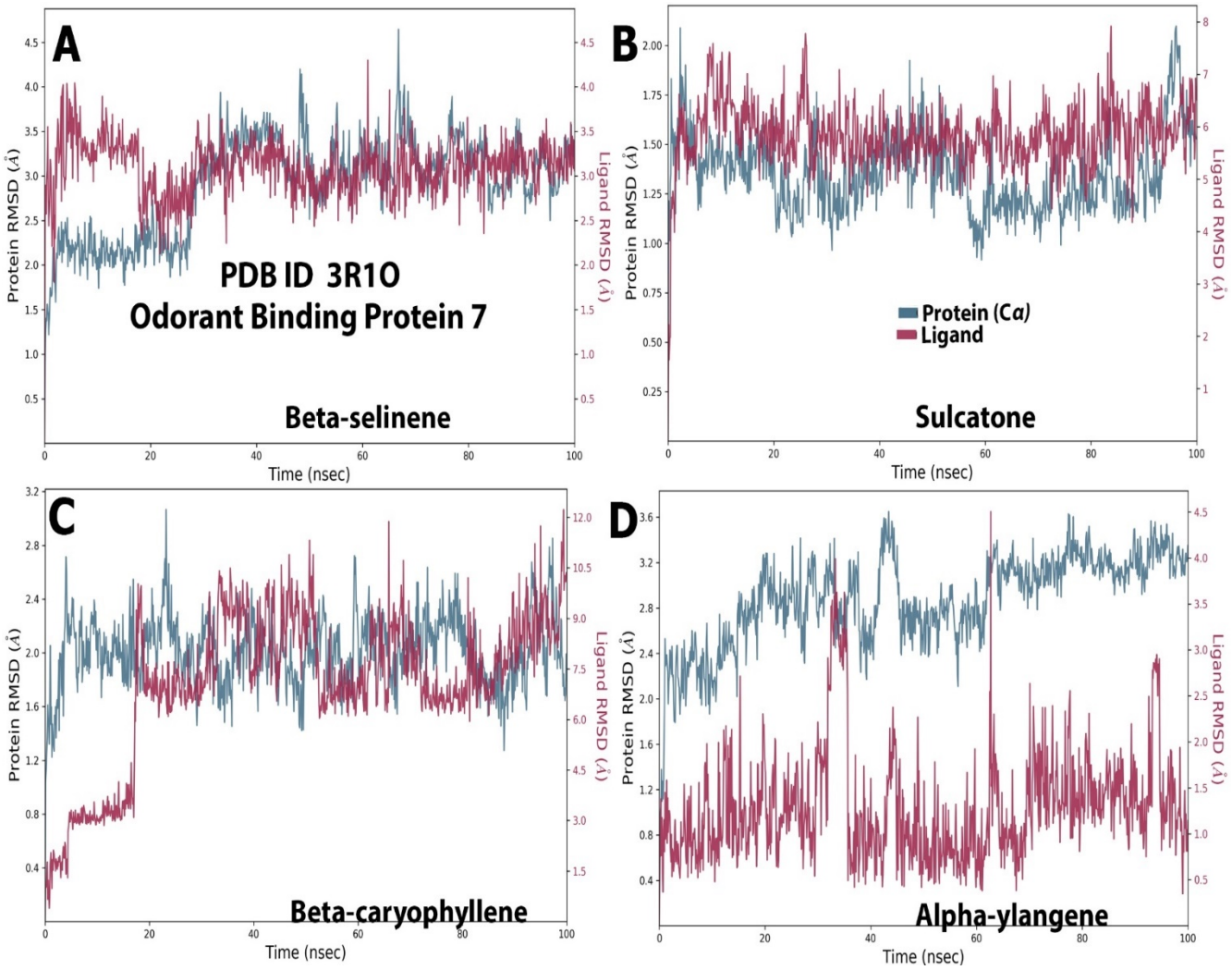

Figure 9. The RMSD of the odorant-binding protein 7 complexed the lead phytochemicals (**A**–**D**) in the selected trajectory across the MD simulation period of 100 ns.

3.14. Response of A. gambiae to the Essential Oil and Selected Compounds

Figure 10 indicates five ligands identified in the V.negundo essential oil, and these results are reported in Table S1. Figures 3–5 depict the behavioral responses of the 150 female *A. gambiae* to the *V. negundo* oil, positive control (DEET), and pure compounds.

The observed repellency of the essential oil compared to the chemical-based repellent underlines the potency of the oil, which is in tandem with the ethno-application of the *V. negundo* as a mosquito repellent as reported by Hazarika et al. [55] and Zaidan et al. [56].

As the exposure time increases, the repellency activity of the compounds increases to a concentration where there are no observable changes in activity. The essential oil showed a significant increase in the percentage of mosquitoes repelled at 49.9 min compared to the compounds; however, no significant difference ($p > 0.05$) was observed in the percentage of mosquitoes repelled between the pure compounds.

The contact time of the tested samples varied depending on their diffusivity (Figures 3–5); in the first 10 min of exposure to *V. negundo* oil and DEET, they repelled about 76% and 85%

of the *A. gambiae* (Figure 11a,b, while 24%, 18%, 14%, and 19% of the *A. gambiae* responded to the presence of β-selinene, β-caryophellene, sulcatone, and α-ylangene, respectively (Figure 11c–f).

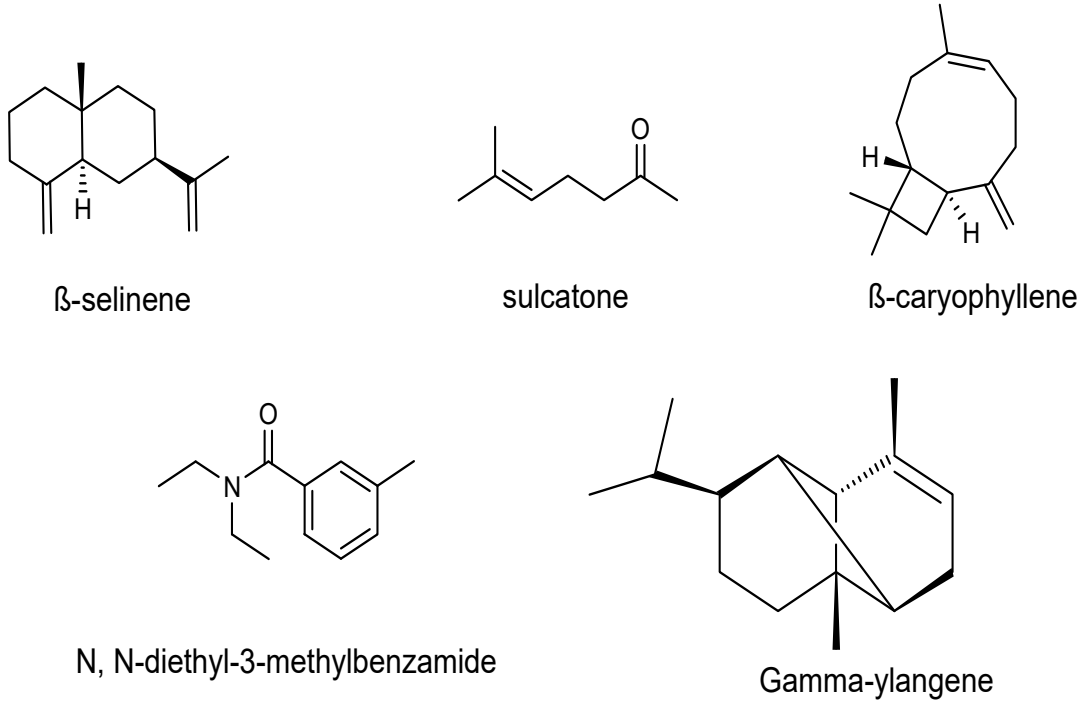

Figure 10. Two-dimensional structures of the selected ligands and positive control (N,N-diethyl-3-methylbenzamide).

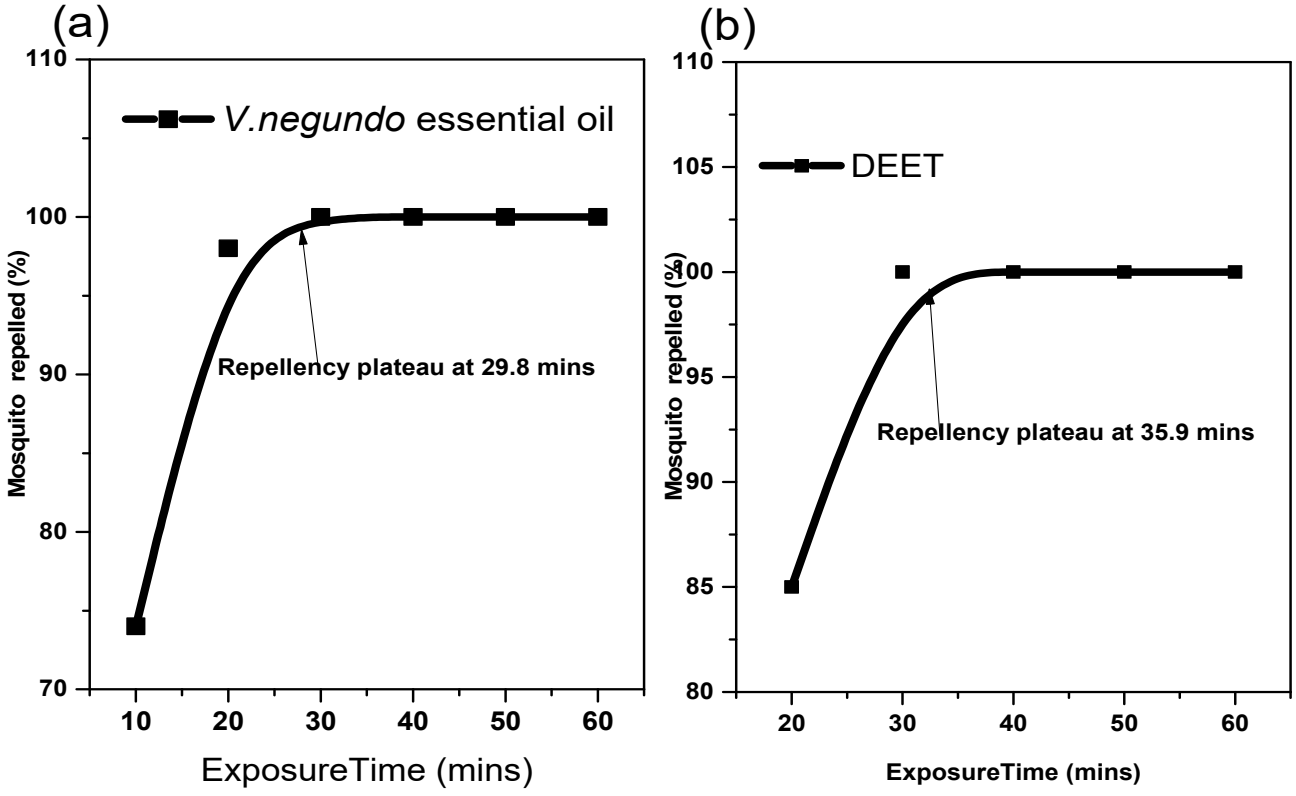

Figure 11. *Cont.*

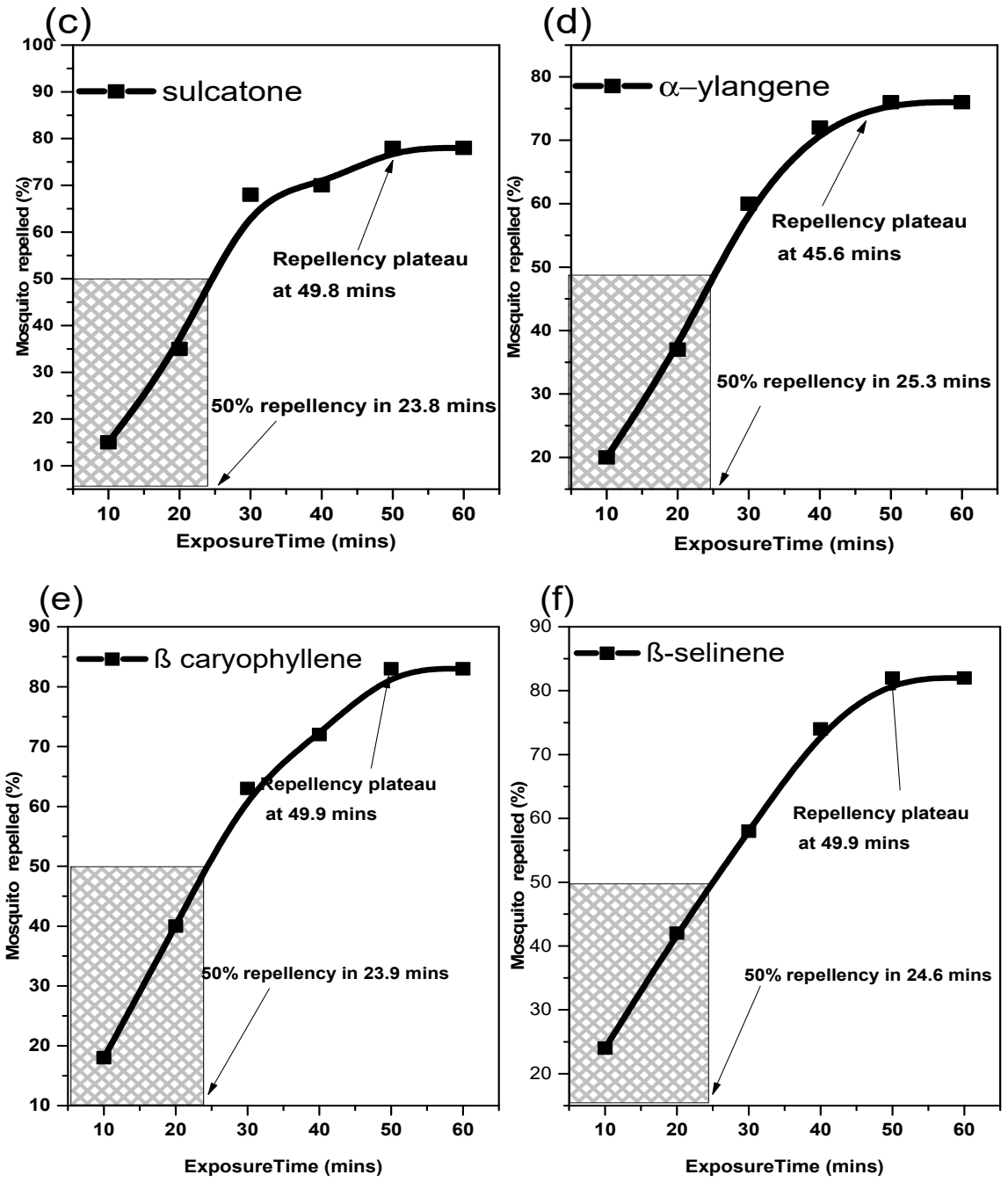

Figure 11. Percentage mosquito repelled by (**a**) 0.48% *v*/*v V. negundo* essential oil and (**b**) 0.01% *v*/*v* DEET: N,N-diethyl-3-methylbenzamide after 60 min exposure, (**c**) sulcatone (**d**) α-ylangene after 60 min exposure, (**e**) β-caryophellene, and (**f**) β-selinene after 60 min exposure.

In 60 min, sulcatone, α-ylangene, β-caryophellene, and β-selinene, repelled 75%, 77%, 85%, and 83%, while the oil and DEET repelled 100% of the *A. gambiae.* There is a significant difference in the responses of the *A. gambiae* to the oil and DEET compared to the pure compounds (Figure 11c–f). The optimal repellencies of the oil and DEET were recorded at 29.8 min and 35.9 min. Pure compounds showed an increase in the amount of mosquitoes repelled with time, with an optimal % repellency activity attained at approximately 45.6–49.9 min.

However, the sensitivities of the *A. gambiae* to the test compounds vary slightly, with *A. gambiae* being most and least sensitive to sulcatone at 15 min and β-selinene at about 26.7 min. Further, the time required to repel 50% of the *A. gambiae* varies from one pure

compound to another. Sulcatone and β-caryophellene showed 50% repellency activity in the shortest time of 23.9 min, contrary to the observed repellency of α-ylangene at 25.3 min. Sulcatone has been reported to be potent against *Drosophila melanogaster* and *Toxorhynchites amboinensis* [57]. This inference is in consonance with the studies of Angraeni et al. [58] and Nararak et al. [59,60].

Most insect repellents, including DEET, have a species-specific method of action that is sometimes unknown. Activation of specific odorant receptors (ORs), inhibition of specific ORs, and modulation of multiple ORs, according to Tsitoura et al. [34] and Degennaro et al. [61], may be suggestive of functional blocking of the olfactory receptor co-receptor, resulting in *A. gambiae* susceptibility to the molecules in the repellent.

4. Conclusions

The essential oil of *V. negundo* showed significant mosquito repellent efficacy ($p < 0.05$) when compared to DEET, with optimal repellency achieved in 29.8 min versus 35.7 min for DEET. According to the docking studies, four phytocompounds (β-selinene, β-caryophellene, sulcatone, and α-ylangene) showed decreased activity when tested individually, with an average optimal repellency time of 48.25 min. This decrease in activity is due to the loss of synergism. The ligand efficiency values were all within the expected ranges, implying that the ligands were quantitatively hit and thus qualify as a potential odorant-binding protein repellent lead. Among the lead phytochemicals, β-selinene displayed a multiplicity of highest binding tendencies to three of the OBPs (OBP 1, OBP 4, and OBP). β-selinene, in part or in association with the four lead phytochemicals, may be involved in the functional blocking of the olfactory receptors and co-receptors, which underlines the repellant activities of the essential oil from *A. gambiae*. The complexes formed between the lead phytocompounds and the OBP 7 were stable in the dynamic environment, hence can be adapted for further wet experimental studies. Based on these findings, *V. negundo* oil can be used in a variety of ways to enhance or replace repellent agents in traditional repellents. It can also be used as a natural anti-mosquito agent in the preparation of aerosol, repellent lotion, and repellent fabrics.

Supplementary Materials: The following supporting information can be downloaded at: https://www.mdpi.com/article/10.3390/app12157500/s1, Plate S1. Lane M is the 100bp marker, Lane 1–20 are randomly selected Anopheles samples. Lane 21 = negative Sample. Distinguishing band size: *Anopheles gambiae* s.l at 390bp; Anopheles arabiensis 315 bp; Plate S2. Agarose gel 1.5% for distinguishing *An. gambiae* s.s and coluzzi after PCR with primers (R3, R5, B/Sint & MoPint). Lane M = 100bp molecular weight marker; visible at 500 bp and 1000 bp. Samples 1 to 7 are *Anopheles gambiae* s.l randomly picked from a group of 20 in Kaduna and shows DNA band sizes of 475bp to authenticate species to be *Anopheles gambiae* s.s, Figure S1: Chromatogram of *V. negundo* essential oil, Figure S2: Ligand properties of β-selinene, Figure S3: Ligand properties of β-caryophellene, Figure S4: Ligand properties of sulcatone, and Figure S5: Ligand properties of α-ylangene complexed with odorant binding protein 7 across a 100 ns MD simulation (a) Ligand RMSD (b) Radius of Gyration (rGyr) (c) Intramolecular Hydrogen Bonds (intraHB) (d) Molecular Surface Area (MolSA) (e) Solvent Accessible Surface Area (SASA) (f) Polar Surface Area (PSA), Table S1: Molecular docking results for the interaction between the ligands and the target proteins, and Table S2: Global reactivity descriptors of the FLP.

Author Contributions: Conceptualization, B.J.O., W.A.E., Z.L., J.C.O. and M.A.; Data curation, W.A.E. and A.R.G.; Formal analysis, W.A.E. and A.R.G.; Funding acquisition, B.J.O. and Z.L.; Investigation, B.J.O., Z.L. and J.C.O.; Methodology, B.J.O., G.A.G., Z.L. and M.A.; Project administration, B.J.O.; Resources, Z.L.; Software, W.A.E., G.A.G., A.R.G. and M.A.; Supervision, Z.L.; Validation, G.A.G.; Visualization, A.R.G.; Writing—original draft, B.J.O., G.A.G. and, J.C.O.; Writing—review & editing, B.J.O. and G.A.G. All authors have read and agreed to the published version of the manuscript.

Funding: This research was funded by the Tertiary Education Trust Fund, grant number TETFund/DR&D/CE/NRF/UNI/CC/22, and the APC was funded by the Tertiary Education Trust Fund.

Institutional Review Board Statement: Not applicable.

Informed Consent Statement: Not applicable.

Data Availability Statement: The data used to support this study are available within the manuscript.

Acknowledgments: We appreciate the School of Pharmaceutical Sciences, Cheeloo College of Medicine, Shandong University, China, Kaduna State University, Kaduna State, Nigeria, and Bingham University, Karu, Nasarawa State, Nigeria, for providing the necessary environment for this collaborative investigation.

Conflicts of Interest: The authors have declared that there is no conflict of interest.

References

1. Wickremasinghe, R.; Wickremasinghe, A.R.; Fernando, S.D. Climate change and malaria a complex relationship. *UN Chron.* **2012**, *47*, 21–25. [CrossRef]
2. Müller, P.; Pflüger, V.; Wittwer, M.; Ziegler, D.; Chandre, F.; Simard, F.; Lengeler, C. Identification of Cryptic Anopheles Species by Molecular Protein Profiling. *PLoS ONE* **2013**, *8*, e57486. [CrossRef]
3. Omumbo, R.W.S.; Malaria, J.A. *Disease and Mortality in Sub-Saharan Africa*, 2nd ed.; Jamison, D.T., Feachem, R.G., Makgoba, M.W., Bos, E.R., Baingana, F.K., Hofman, K.J., Rogo, K.O., Eds.; World Bank: Washington, DC, USA, 2006.
4. World Health Organization. *World Health Organization More Pregnant Women and Children Protected from Malaria, but Accelerated Efforts and Funding Needed to Reinvigorate Global Response*; World Health Organization: Geneva, Switzerland, 2019.
5. Weiss, D.J.; Bertozzi-Villa, A.; Rumisha, S.F.; Amratia, P.; Arambepola, R.; Battle, K.E.; Cameron, E.; Chestnutt, E.; Gibson, H.S.; Harris, J.; et al. Indirect effects of the COVID-19 pandemic on malaria intervention coverage, morbidity, and mortality in Africa: A geospatial modelling analysis. *Lancet Infect. Dis.* **2021**, *21*, 59–69. [CrossRef]
6. World Health Organization. *WHO Malaria*; World Health Organization: Geneva, Switzerland, 2022.
7. Tinto, H.; Otieno, W.; Gesase, S.; Sorgho, H.; Otieno, L.; Liheluka, E.; Valéa, I.; Sing'oei, V.; Malabeja, A.; Valia, D.; et al. Long-term incidence of severe malaria following RTS,S/AS01 vaccination in children and infants in Africa: An open-label 3-year extension study of a phase 3 randomised controlled trial. *Lancet Infect. Dis.* **2019**, *19*, 821–832. [CrossRef]
8. Pryce, J.; Medley, N.; Choi, L. Indoor residual spraying for preventing malaria in communities using insecticide-treated nets. *Cochrane Database Syst. Rev.* **2022**, *2022*, CD012688. [CrossRef]
9. Plowe, C.V. Malaria chemoprevention and drug resistance: A review of the literature and policy implications. *Malar. J.* **2022**, *21*, 1–25. [CrossRef]
10. Hemingway, J.; Shretta, R.; Wells, T.N.C.; Bell, D.; Djimdé, A.A.; Achee, N.; Qi, G. Tools and Strategies for Malaria Control and Elimination: What Do We Need to Achieve a Grand Convergence in Malaria? *PLoS Biol.* **2016**, *14*, e1002380. [CrossRef]
11. Riveron, J.M.; Tchouakui, M.; Mugenzi, L.; Menze, B.D.; Chiang, M.-C.; Wondji, C.S. Insecticide Resistance in Malaria Vectors: An Update at a Global Scale. In *Towards Malaria Elimination—A Leap Forward*; InTech Open: Rijeka, Croatia, 2018.
12. World Health Organization. *WHO Insecticide Resistance-Global Malaria Programme*; World Health Organization: Geneva, Switzerland, 2021.
13. Matiya, D.J.; Philbert, A.B.; Kidima, W.; Matowo, J.J. Dynamics and monitoring of insecticide resistance in malaria vectors across mainland Tanzania from 1997 to 2017: A systematic review. *Malar. J.* **2019**, *18*, 102. [CrossRef]
14. Fodjo, B.K.; Koudou, B.G.; Tia, E.; Saric, J.; N'Dri, P.B.; Zoh, M.G.; Gba, C.S.; Kropf, A.; Kesse, N.B.; Chouaïbou, M.S. Insecticides Resistance Status of An. gambiae in Areas of Varying Agrochemical Use in Côte D'Ivoire. *Biomed. Res. Int.* **2018**, *2018*, 2874160. [CrossRef]
15. Shah, N.K.; Valecha, N. Antimalarial drug resistance. *Recent Adv. Malar.* **2016**, *10*, 383–407. [CrossRef]
16. Benelli, G.; Jeffries, C.L.; Walker, T. Biological control of mosquito vectors: Past, present, and future. *Insects* **2016**, *7*, 52. [CrossRef] [PubMed]
17. Wheelwright, M.; Whittle, C.R.; Riabinina, O. Olfactory systems across mosquito species. *Cell Tissue Res.* **2021**, *383*, 75–90. [CrossRef] [PubMed]
18. Zafar, Z.; Fatima, S.; Bhatti, M.F.; Shah, F.A.; Saud, Z.; Butt, T.M. Odorant Binding Proteins (OBPs) and Odorant Receptors (ORs) of Anopheles stephensi: Identification and comparative insights. *PLoS ONE* **2022**, *17*, e0265896. [CrossRef] [PubMed]
19. Scieuzo, C.; Nardiello, M.; Farina, D.; Scala, A.; Cammack, J.A.; Tomberlin, J.K.; Vogel, H.; Salvia, R.; Persaud, K.; Falabella, P. *Hermetia illucens* (L.) (diptera: Stratiomyidae) odorant binding proteins and their interactions with selected volatile organic compounds: An in silico approach. *Insects* **2021**, *12*, 814. [CrossRef]
20. Smith, M.B.; March, J. *March's Advanced Organic Chemistry: Reactions, Mechanisms, and Structure*, 5th ed.; Sixth; John Wiley & Sons, Inc.: Hoboken, NJ, USA, 2001; Volume 6, ISBN 9780471720911.
21. Rihani, K.; Ferveur, J.F.; Briand, L. The 40-year mystery of insect odorant-binding proteins. *Biomolecules* **2021**, *11*, 509. [CrossRef] [PubMed]
22. Guo, W.; Ren, D.; Zhao, L.; Jiang, F.; Song, J.; Wang, X.; Kang, L. Identification of Odorant-Binding Proteins (OBPs) and functional analysis of phase-related OBPs in the migratory locust. *Front. Physiol.* **2018**, *9*, 984. [CrossRef]

23. da Costa, K.S.; Galúcio, J.M.; da Costa, C.H.S.; Santana, A.R.; Carvalho, V.D.S.; do Nascimento, L.D.; Lima e Lima, A.H.; Cruz, J.N.; Alves, C.N.; Lameira, J. Exploring the Potentiality of Natural Products from Essential Oils as Inhibitors of Odorant-Binding Proteins: A Structure- and Ligand-Based Virtual Screening Approach to Find Novel Mosquito Repellents. *ACS Omega* **2019**, *4*, 2475–22486. [CrossRef]
24. Ullah, Z.; Ullah, R.; Shah, A.-H.A.; Ahmad, I.; Haider, S. Phytochemical and Biological Evaluation of Vitex Negundo Linn: A Review. *Int. J. Pharm. Pharm. Sci.* **2012**, *3*, 2421–2431.
25. Singh; Sharma, P.; Garg, V.; Visht, S. Extraction and analysis of essential oil of Nirgundi (*Vitex negundo* L.). *Der Pharm. Sin.* **2011**, *2*, 262–266.
26. Ramirez, J.; Garver, L.; Dimopoulos, G. Challenges and Approaches for Mosquito Targeted Malaria Control. *Curr. Mol. Med.* **2009**, *9*, 116–130. [CrossRef]
27. Kapetanovic, I.M. Computer-Aided Drug Discovery and Development (CADDD): In Silico-Chemico-Biological Approach. *Chem. Biol. Interact.* **2008**, *171*, 165–176. [CrossRef] [PubMed]
28. Maria Antony, D.J.E.; Anoop, M.N. Virtual screening and lead optimisation to identify novel inhibitors for HDAC-8. *arXiv* **2012**, arXiv:1209.2793.
29. Zhang, S. Computer-Aided Drug Discovery and Development. In *Methods in Molecular Biology*; Human Press: Totowa, NJ, USA, 2011.
30. Okoli, B.J.; Ladan, Z.; Mtunzi, F.; Hosea, Y.C. Vitex negundo, L. Essential oil: Odorant binding protein efficiency using molecular docking approach and studies of the mosquito repellent. *Insects* **2021**, *12*, 1061. [CrossRef] [PubMed]
31. Khokra, S.; Prakash, O.; Jain, S.; Aneja, K.; Dhingra, Y. Essential oil composition and antibacterial studies of Vitex negundo Linn. extracts. *Indian J. Pharm. Sci.* **2008**, *70*, 522–526. [CrossRef] [PubMed]
32. Padalia, R.C.; Verma, R.S.; Chauhan, A.; Chanotiya, C.S.; Thul, S. Phytochemical diversity in essential oil of *Vitex negundo* L. populations from India. *Rec. Nat. Prod.* **2016**, *10*, 452–464.
33. Wang, G.; Carey, A.F.; Carlson, J.R.; Zwiebel, L.J. Molecular basis of odor coding in the malaria vector mosquito Anopheles gambiae. *Proc. Natl. Acad. Sci. USA* **2010**, *107*, 4418–4423. [CrossRef]
34. Tsitoura, P.; Koussis, K.; Iatrou, K. Inhibition of Anopheles gambiae odorant receptor function by mosquito repellents. *J. Biol. Chem.* **2015**, *290*, 7961–7972. [CrossRef]
35. Xu, P.; Choo, Y.M.; De La Rosa, A.; Leal, W.S. Mosquito odorant receptor for DEET and methyl jasmonate. *Proc. Natl. Acad. Sci. USA* **2014**, *111*, 16592–16597. [CrossRef]
36. Bohbot, J.D.; Dickens, J.C. Odorant receptor modulation: Ternary paradigm for mode of action of insect repellents. *Neuropharmacology* **2012**, *62*, 2086–2095. [CrossRef]
37. Martyna, G.J.; Klein, M.L.; Tuckerman, M. Nosé-Hoover chains: The canonical ensemble via continuous dynamics. *J. Chem. Phys.* **1992**, *97*, 2635–2643. [CrossRef]
38. Coetzee, M. Key to the females of Afrotropical Anopheles mosquitoes (Diptera: Culicidae). *Malar. J.* **2020**, *19*, 70. [CrossRef] [PubMed]
39. Achee, N.L.; Grieco, J.P.; Moore, S.; Bernier, U. *Guidelines for Efficacy Testing of Spatial Repellents*; WHO: Geneva, Switzerland, 2013; pp. 5–7; 14–15; 28–30; 41–48.
40. Badolo, A.; Ilboudo-Sanogo, E.; Ouédraogo, A.P.; Costantini, C. Evaluation of the sensitivity of Aedes aegypti and Anopheles gambiae complex mosquitoes to two insect repellents: DEET and KBR 3023. *Trop. Med. Int. Health* **2004**, *9*, 330–334. [CrossRef] [PubMed]
41. Maniafu, B.M.; Wilber, L.; Ndiege, I.O.; Wanjala, C.C.; Akenga, T.A. Larvicidal activity of extracts from three Plumbago spp against Anopheles gambiae. *Mem. Inst. Oswaldo Cruz* **2009**, *104*, 813–817. [CrossRef]
42. Gill, B.S.; Mehra, R.; Navgeet; Kumar, S. Vitex negundo and its medicinal value. *Mol. Biol. Rep.* **2018**, *45*, 2925–2934. [CrossRef] [PubMed]
43. Huang, H.C.; Chang, T.Y.; Chang, L.Z.; Wang, H.F.; Yih, K.H.; Hsieh, W.Y.; Chang, T.M. Inhibition of melanogenesis Versus antioxidant properties of essential oil extracted from leaves of vitex negundo linn and chemical composition analysis by GC-MS. *Molecules* **2012**, *17*, 3902–3916. [CrossRef] [PubMed]
44. Bonjardim, L.R.; Cunha, E.S.; Guimarães, A.G.; Santana, M.F.; Oliveira, M.G.B.; Serafini, M.R.; Araújo, A.A.S.; Antoniolli, Â.R.; Cavalcanti, S.C.H.; Santos, M.R.V.; et al. Evaluation of the anti-inflammatory and antinociceptive properties of p-Cymene in mice. *Z. Nat. Sect. C J. Biosci.* **2012**, *67*, 15–21. [CrossRef]
45. Conti, B.; Benelli, G.; Flamini, G.; Cioni, P.L.; Profeti, R.; Ceccarini, L.; Macchia, M.; Canale, A. Larvicidal and repellent activity of *Hyptis suaveolens* (Lamiaceae) essential oil against the mosquito *Aedes albopictus* Skuse (Diptera: Culicidae). *Parasitol. Res.* **2012**, *110*, 2013–2021. [CrossRef]
46. Kim, J.-K.; Kang, C.-S.; Lee, J.-K.; Kim, Y.-R.; Han, H.-Y.; Yun, H.K. Evaluation of Repellency Effect of Two Natural Aroma Mosquito Repellent Compounds, Citronella and Citronellal. *Entomol. Res.* **2005**, *35*, 117–120. [CrossRef]
47. Rana, V.S.; Dayal, R. Seasonal variation of the essential oil of Vitex negundo leaves. *Indian For.* **2003**, *129*, 607–610.
48. Schultes, S.; De Graaf, C.; Haaksma, E.E.J.; De Esch, I.J.P.; Leurs, R.; Krämer, O. Ligand efficiency as a guide in fragment hit selection and optimization. *Drug Discov. Today Technol.* **2010**, *7*, e157–e162. [CrossRef]
49. Murray, C.W.; Erlanson, D.A.; Hopkins, A.L.; Keserü, G.M.; Leeson, P.D.; Rees, D.C.; Reynolds, C.H.; Richmond, N.J. Validity of ligand efficiency metrics. *ACS Med. Chem. Lett.* **2014**, *5*, 616–618. [CrossRef] [PubMed]

50. Padmanabhan, J.; Parthasarathi, R.; Subramanian, V.; Chattaraj, P.K. Molecular structure, reactivity, and toxicity of the complete series of chlorinated benzenes. *J. Phys. Chem. A* **2005**, *109*, 11043–11049. [CrossRef] [PubMed]
51. Amine, K.; Miri, L.; Naimi, A.; Saile, R.; El Kharrim, A.; Mikou, A.; Kettani, A. Molecular dynamics approach in the comparison of wild-type and mutant paraoxonase-1 apoenzyme form. *Bioinform. Biol. Insights* **2015**, *9*, 129–140. [CrossRef]
52. Sinha, S.; Wang, S.M. Classification of VUS and unclassified variants in BRCA1 BRCT repeats by molecular dynamics simulation. *Comput. Struct. Biotechnol. J.* **2020**, *18*, 723–736. [CrossRef] [PubMed]
53. Xiaolin, C.; Ivanov, I. Molecular dynamics. *Methods Mol. Biol.* **2012**, *278*, 585–586. [CrossRef]
54. Ogunyemi, O.M.; Gyebi, G.A.; Elfiky, A.A.; Afolabi, S.O.; Ogunro, O.B.; Adegunloye, A.P.; Ibrahim, I.M. Alkaloids and flavonoids from African phytochemicals as potential inhibitors of SARS-Cov-2 RNA-dependent RNA polymerase: An in silico perspective. *Antivir. Chem. Chemother.* **2020**, *28*, 2040206620984076. [CrossRef]
55. Hazarika; Dhiman, S.; Rabha, B.; Bhola, R.; Singh, L. Repellent activity of some essential oils against simulium species in India. *J. Insect Sci.* **2012**, *12*, 501. [CrossRef]
56. Zaidan, M.R.; Noor Rain, A.; Badrul, A.R.; Adlin, A.; Norazah, A.; Zakiah, I. In vitro screening of five local medicinal plants for antibacterial activity using disc diffusion method. *Trop. Biomed.* **2005**, *22*, 165–170.
57. Dekel, A.; Yakir, E.; Bohbot, J.D. The sulcatone receptor of the strict nectar-feeding mosquito Toxorhynchites amboinensis. *Insect Biochem. Mol. Biol.* **2019**, *111*, 103174. [CrossRef]
58. Anggraeni, T.; Nisrine, N.; Barlian, A.; Sumarsono, S.H. Repellency of some essential oils against Drosophila melanogaster, vector for bacterium blood disease in banana plantation. *J. Entomol.* **2018**, *15*, 125–134. [CrossRef]
59. Nararak, J.; Di Giorgio, C.; Sukkanon, C.; Mahiou-Leddet, V.; Ollivier, E.; Manguin, S.; Chareonviriyaphap, T. Excito-repellency and biological safety of β-caryophyllene oxide against *Aedes albopictus* and *Anopheles dirus* (Diptera: Culicidae). *Acta Trop.* **2020**, *210*, 105556. [CrossRef] [PubMed]
60. Nararak, J.; Sathantriphop, S.; Kongmee, M.; Mahiou-Leddet, V.; Ollivier, E.; Manguin, S.; Chareonviriyaphap, T. Excito-repellent activity of β-caryophyllene oxide against Aedes aegypti and *Anopheles minimus*. *Acta Trop.* **2019**, *197*, 105030. [CrossRef] [PubMed]
61. Degennaro, M.; McBride, C.S.; Seeholzer, L.; Nakagawa, T.; Dennis, E.J.; Goldman, C.; Jasinskiene, N.; James, A.A.; Vosshall, L.B. Orco mutant mosquitoes lose strong preference for humans and are not repelled by volatile DEET. *Nature* **2013**, *498*, 487–491. [CrossRef] [PubMed]